Journal of Electrostatics 70 (2012) 374–383

Contents lists available at SciVerse ScienceDirect

Journal of Electrostatics

journal homepage: www.elsevier.com/locate/elstat

An analytical approach to wire-to-cylinder corona discharge

K. Yanallah [a,*], F. Pontiga [b], Y. Meslem [a], A. Castellanos [b]

[a] Laboratoire de génie électrique et des plasmas, Université de Tiaret, Algeria
[b] Universidad de Sevilla, Sevilla, Spain

ARTICLE INFO

Article history:
Received 8 August 2011
Received in revised form
19 March 2012
Accepted 9 May 2012
Available online 26 May 2012

Keywords:
Corona discharge
Analytic approach
Chemical reactions
Ozone generation

ABSTRACT

In the present paper, an analytical approach is proposed to determine the radial distributions of electric field, electrons, ion densities and temperature of a DC corona discharge in wire-to-cylinder geometry, using oxygen as feed gas. The current–voltage (CV) characteristic measured in experiments is used as an input in the calculation. The objective of this work is to provide approximated analytical solutions of the corona discharge with low computational cost, which can be useful in different technological applications, such as the generation of ozone or the decomposition of pollutant gases. The predictions of the analytical model are compared with the results obtained from a much more complete numerical simulation.

1. Introduction

Corona discharge is initiated when a sufficiently high voltage is applied to an electrode with a small radius of curvature, usually a point, a wire or a blade. The electric field is strongly reinforced in the vicinity of the stressed electrode, and free electrons generated by natural background radiation are accelerated by the electric field towards the anode. If they gain sufficient energy, they can ionize new molecules, thus producing more positive ions and electrons. Electrons can also attach to neutral molecules to form negative ions or to initiate electron-induced reactions that may generate radicals. The polarity of corona discharge is determined by the sign of the voltage applied to the stressed electrode. Of course, the motion of charged particles is different in positive and negative polarities, and this has important consequences on the characteristics of the electrical discharge. In positive polarity, electrons and negative ions drift towards the point, wire or blade. Therefore, the ionization region in positive corona is significantly smaller than in the case of negative corona.

The applications of corona discharge have known a steady growth in industrial and technological applications, such as the decomposition of gaseous pollutants, the sterilization of water, the surface treatment of polymer films, the production of ozone, etc. [1–7]. In pure oxygen, ozone is the most important molecule generated by corona discharge. As it is well known, this molecule is generated following a two-step process [8]:

(i) Free radicals of oxygen are generated by direct dissociation of molecular oxygen,

$$e + O_2 \rightarrow O + O + e. \quad (R1)$$

(ii) Ozone is then produced via a three-body reaction:

$$O + O_2 + O_2 \rightarrow O_3 + O_2. \quad (R2)$$

Consequently, the knowledge of the electron density distribution and of the reaction rate coefficient (R1), which depends on the electric field strength, is essential to evaluate the radial distribution of atomic oxygen, and to quantify the ozone generated through reaction (R2), which is also temperature dependent. The development of many other plasma-based applications requires as well a precise knowledge of the spatial distribution of charged particles, electric field and temperature.

Many numerical studies have been carried out in the past to determine these parameters [9–17]. For example, Pontiga et al. [9] studied the generation of ozone by computing the spatial distribution of the species generated in a wire-cylinder corona discharge in pure oxygen using different plasma chemistry models. The numerical model of Chen et al. [10] for ozone generation by positive DC corona discharges in dry air combined the physical processes in the corona discharge with the chemistry of ozone formation and

* Corresponding author.
E-mail addresses: yanallahkh@yahoo.fr, yanallahkh@gmail.com (K. Yanallah).

0304-3886/$ – see front matter © 2012 Elsevier B.V. All rights reserved.
doi:10.1016/j.elstat.2012.05.002

destruction in the air stream. They solved the continuity equation of the charged and the neutral particles separately. For a different electrode geometry, Adamiak and Atten [12] presented a numerical model to determine the distributions of electric field and charge density in point–plane positive corona discharge. In general, all these investigations are based on the numerical resolution of the nonlinear coupled differential equations that govern the corona discharge. Much fewer studies have tried to obtain approximate analytical solutions of the corona discharge. Stearn [18], for example, analysed the positive corona discharge in coaxial cylindrical geometry for the air gas, by focussing on the electrical discharge properties.

Usually, the exact calculation of the electric field and electron density requires sophisticated modelling and, for that reason, some authors use estimates of these parameters. For instance, Held et al. [19] assume that the electrode gap can be divided in two distinct regions, where either gas ionization or electron attachment is the dominant process. Then, they compute an approximated expression for the mean electron density, which allows them to evaluate analytically the concentration of ozone in an oxygen-fed wire-to-cylinder ozonizer. However, simpler approximations are also used in other studies. For example, Mikoviny et al. [20] have assumed a constant value of electron density in their investigation of corona discharge in pure carbon dioxide and its mixtures with oxygen.

In the present work, the problem of positive and negative corona discharge in pure oxygen without gas flow will be investigated analytically in coaxial wire-to-cylinder geometry using some plausible approximations. The spatial distribution of charged particles, electric field and temperature will then be obtained by solving separately Poisson's equation, the continuity equations of charged particles and the heat equation, and taking in account the principal physical and chemical processes of corona discharge. The experimental current–voltage (CV) characteristic of the corona discharge will be used in the analytical resolution. In contrast with a complete numerical simulation, the proposed solutions can be evaluated in a negligible computational time, and may be useful as a starting point for the modelling of the generation of ozone and other radicals in corona discharge reactors. This work is a continuation of previous numerical studies developed by the authors in the field of ozone generation by corona discharge [15,17].

The paper is organized as follows. Firstly, a brief description of the experimental setup is presented. Then, the governing equations of positive and negative corona discharge that have been solved in the complete numerical model are discussed. The results section is divided in two subsections, for positive and negative polarity respectively, at it is devoted to describing the analytic model and discussing the different approximations.

2. Experimental set-up

The corona discharge reactor used in the experiments consisted of a wire-to-cylinder coaxial electrode system, as shown schematically in Fig. 1. The corona wire was made from tungsten, with radius $r_0 = 62.5$ μm, and the cylinder was made from stainless steel, with radii $R = 1.1$ cm. Both the wire and the cylinder have identical length, $L = 5$ cm. The cylinders were closed with a pair of PVC insulating caps that included parallel windows to allow observation. The reactor was filled with high purity oxygen (99.995%) at atmospheric pressure and room temperature. Positive or negative DC high voltage was applied to the wire with an HV amplifier (Trek 610C), while the cylinder was connected to ground through a digital multimeter (Keithley 196). Each voltage was applied for about 45 min. Fig. 2 shows the measured current–voltage characteristic corresponding to both polarities of the corona discharge.

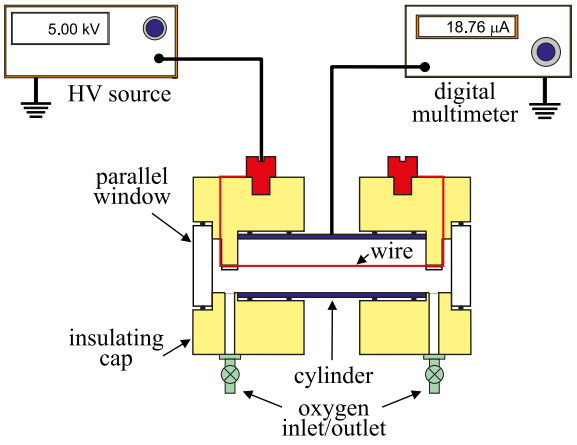

Fig. 1. Schematic of the experimental apparatus used in the experiments.

3. Governing equations

Positive and negative corona discharge in wire-to-cylinder geometry can be numerically simulated using a fluid model approximation, namely a continuity equation for each species density, coupled with Gauss equation for the electric field and the energy conservation equation for the gas temperature. Assuming a stationary discharge, the continuity equations governing the number density of the i-th charged species, N_i^c, and of the j-th neutral species, N_j, can be written in cylindrical coordinates as [16,21,22]

$$\pm\frac{1}{r}\frac{\mathrm{d}}{\mathrm{d}r}\left[r\frac{e_i}{e_0}N_i^c\mu_i E\right] = S_i, \tag{1}$$

$$-\frac{1}{r}\frac{\mathrm{d}}{\mathrm{d}r}\left[rD_j\frac{\mathrm{d}N_j}{\mathrm{d}r}\right] = S_j, \tag{2}$$

where r is the radial distance, e_i and μ_i are the electrical charge and mobility of the charged species, e_0 is the elementary charge ($e_0 \approx 1.602 \times 10^{-19}$ C), D_j is the diffusion coefficient, E is the modulus of the electric field, and S_i and S_j represent the gain/loss balance of these species due to the chemical reactions induced by

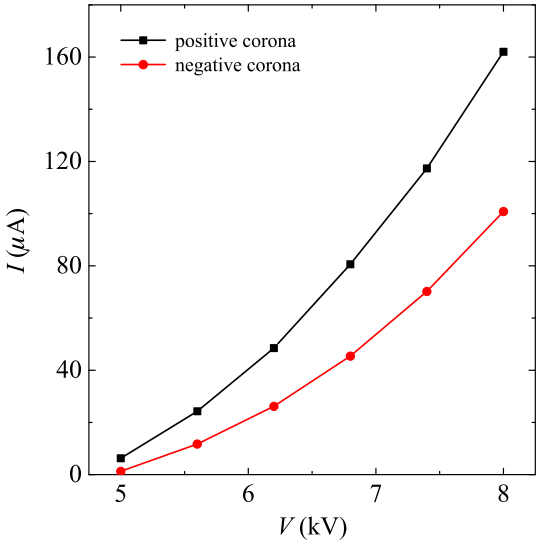

Fig. 2. Current–voltage characteristic of wire-to-cylinder corona discharge.

the electrical discharge. In writing (1) and (2), two basic approximations have been assumed: (i) the electrical discharge possesses rotational symmetry around the wire [18,21], and (ii) the material functions of the gas (drift velocities, reaction rate constants, etc.) are entirely determined by the local reduced electric field E/N, where N is the neutral gas density.

The electric field is modified by the space charge according to Gauss equation,

$$\pm\frac{1}{r}\frac{\mathrm{d}}{\mathrm{d}r}(rE) = \frac{1}{\varepsilon_0}\sum_i e_i N_i^c, \tag{3}$$

where ε_0 is the gas permittivity, and the electric field can be obtained as the gradient of an electrical potential ϕ, $E = -\mathrm{d}\phi/\mathrm{d}r$.

During the electrical discharge, the gas temperature increases due to Joule heating dissipation. Therefore, according to the simplifications already introduced in the continuity equations, the energy equation for the gas temperature, T, can be written as

$$-\frac{1}{r}\frac{\mathrm{d}}{\mathrm{d}r}\left[rk\frac{\mathrm{d}T}{\mathrm{d}r}\right] = EJ_{\mathrm{ion}}, \tag{4}$$

where k is the thermal conductivity of the gas and J is the modulus of the current density. Since the thermal transfer between electrons and gas molecules is very poor, only the ionic current density, J_{ion}, has been considered in the rate of heat dissipation. Other sources of heat generation, such as the heat released/absorbed in chemical reactions, will not be taken into account in this study.

The set of nonlinear differential equations (1)–(4) can be successfully integrated using a finite-difference method with deferred corrections. This task was accomplished in recent past works [15,17], where the spatial distribution of electrons, ions, neutral species and, in particular, ozone, was computed. The chemical kinetics model considered in the numerical simulation consisted of 15 species and 38 chemical reactions, such as electron impact reactions (ionization, electron attachment, excitation, dissociation, etc), reactions between ions and neutral particles (charge transfer, electron detachment) and reactions between neutral molecules and atoms in their ground and excited states. Moreover, the results of the numerical simulation for ozone were compared with the experimental measurement of the averaged ozone density inside the corona reactor at different applied voltages. The numerical results showed an acceptable agreement with the experimental observations. Additional details about the modelling, experiments, and the chemical kinetics of corona discharge in oxygen can be found in the cited references. The spatial distributions of charged species predicted by the numerical simulation are presented in Figs. 3,4, 9, and 10 for positive and negative corona, respectively.

Here, the results of the numerical simulation will be used to justify the approximations that will be made when solving analytically the equations of the corona discharge. Moreover, the solutions of the analytical model will be compared with the exact numerical results. A close agreement between the analytical and numerical results is therefore a guarantee that the evaluation of the ozone density from the analytical results will also be in general agreement with the experimental measurements performed in [15,17].

4. Results and discussion

4.1. Positive corona discharge

A usual approximation in the study of positive corona consists in dividing the inter-electrode space in two regions [10]: the ionization or plasma region, and the unipolar drift region of positive ions. The ionization region extends a very short distance from the corona wire, and it is characterized by an intense electric field. In this region, electrons are accelerated under the effect of electric field and cause the ionization of the neutral molecules in inelastic collisions. Furthermore, secondary electrons produced by the photoionization help to sustain the electrical discharge. A certain fraction of electrons attach to neutral molecules to form negative ions. Beyond the ionization region, the electric field strength is insufficient to produce electrons. Therefore, the positive ions generated in the ionization region drift towards the grounded cylinder. The boundary between the ionization region and the positive drift region is situated where the rate of ionization is equal to the rate of electron attachment.

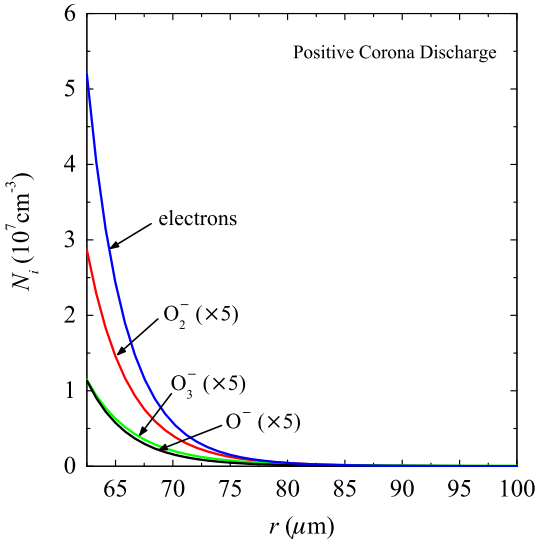

Fig. 3. Radial distribution of electrons and negative ions near the wire (positive corona) for $V = 6.8$ kV, $r_0 = 62.5$ μm and $R = 1.1$ cm (exact numerical solution).

According to the results obtained from the exact numerical solution of (1)–(3), both the ionization region and the positive drift region are dominated by a single species. In the ionization region, electrons are the principal charge carriers (see Fig. 3), since the number density of negative ions, like O_2^-, O_3^- and O^-, are at least one

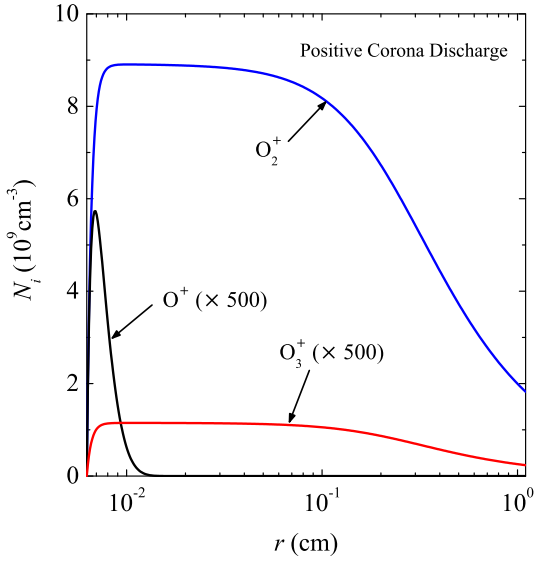

Fig. 4. Radial distribution of positive ions (positive corona) for $V = 6.8$ kV, $r_0 = 62.5$ μm and $R = 1.1$ cm (exact numerical solution).

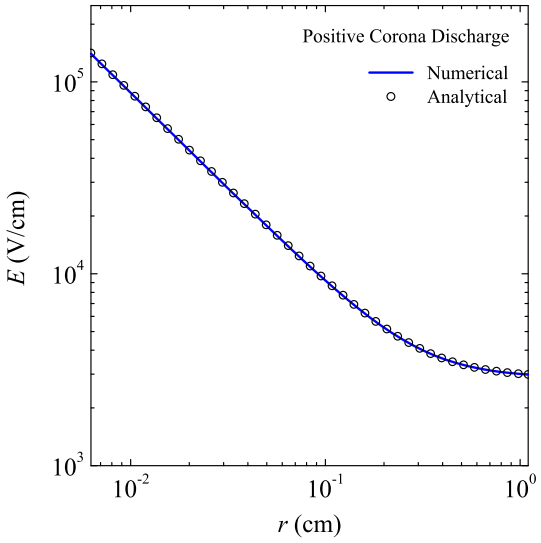

Fig. 5. Radial distribution of the electric field corresponding to $V = 6.2$ kV, $r_0 = 62.5$ μm and $R = 1.1$ cm (positive corona).

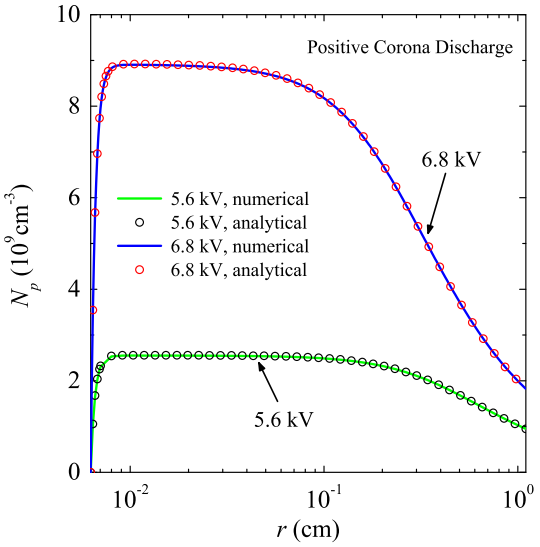

Fig. 7. Radial distribution of the positive ion (O_2^+) density for $r_0 = 62.5$ μm and $R = 1.1$ cm (positive corona).

order of magnitude smaller than electrons. In the positive drift region, O_2^+ is by far the most numerous species (Fig. 4). Therefore, a simplified model with only two charged species (electrons and O_2^+) should reproduce the basic characteristics of the positive corona discharge in oxygen. The governing equations of the positive corona discharge can then be written as

$$-\frac{1}{r}\frac{d}{dr}[rN_e\mu_e E] = (\alpha-\eta)N_e\mu_e E, \tag{5}$$

$$I = 2\pi e_0 rL\left(N_e\mu_e E + N_p\mu_p E\right), \tag{6}$$

$$\frac{1}{r}\frac{d}{dr}[rE] = \frac{e_0}{\varepsilon_0}(N_p - N_e), \tag{7}$$

$$-\frac{1}{r}\frac{d}{dr}\left[rk\frac{dT}{dr}\right] = EJ_{ion}, \tag{8}$$

where N_e and N_p are the number densities of the electron and positive ions (O_2^+), α and η are the ionization and attachment coefficients, respectively, I is the electric current intensity, and μ_e and μ_p denote the mobility of electrons and positive ions. For convenience, the equation for the current intensity (6) will be used instead of the continuity equation to determine the distribution of positive ions.

To our knowledge, the set of coupled nonlinear equations (5)–(8) have not an analytical solution, and its numerical integration is not straightforward. However, as it will be shown in the following sections, some substantial simplifications of the physical problem can still be made, thus facilitating its analytical resolution.

4.1.1. Electric field distribution

In the ionization region, the electric field due to the space charge (Fig. 3) is negligible compared to the applied electric field. Therefore, the total electric field is Laplacian, and satisfies the relation [19]:

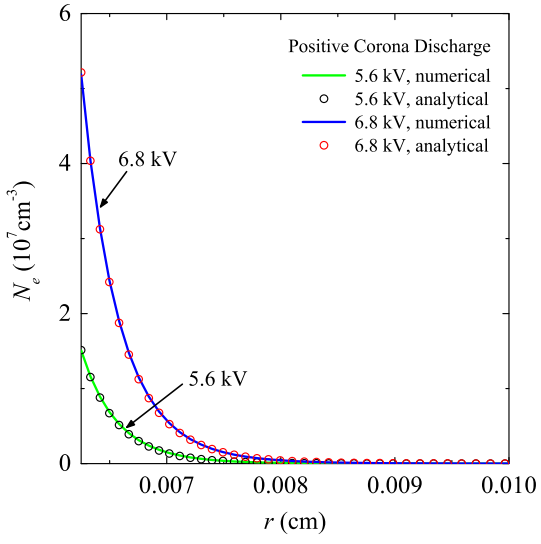

Fig. 6. Radial distribution of the electron density around the wire for $r_0 = 62.5$ μm and $R = 1.1$ cm (positive corona).

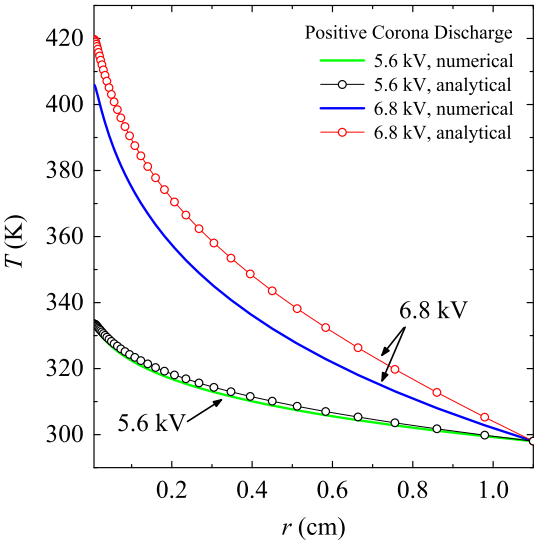

Fig. 8. Radial distribution of temperature corresponding to $r_0 = 62.5$ m and $R = 1.1$ cm (positive corona).

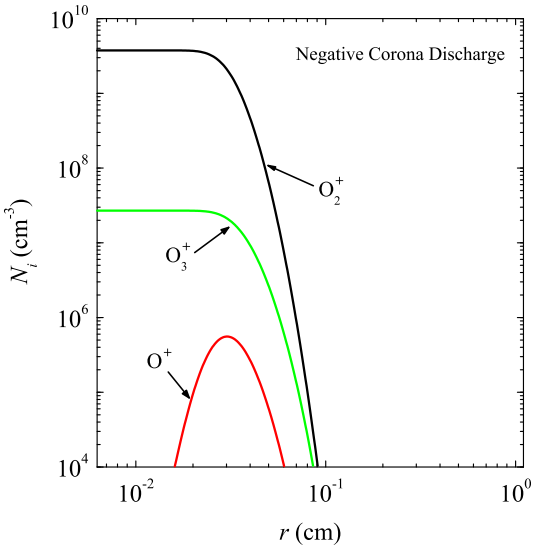

Fig. 9. Radial distribution of positive ions (negative corona) for $V = 6.8$ kV, $r_0 = 62.5$ μm and $R = 1.1$ cm (exact numerical solution).

$$E(r) = \frac{E_0 r_0}{r}, \tag{9}$$

where E_0 is the electric field on the surface of the wire. In contrast, the positive space charge is very important in the drift region (Fig. 4), and reinforces the applied field. Therefore, the electric field on wire will be smaller than the corresponding harmonic electric field,

$$E_h(r_0) = \frac{V}{r_0 \ln\left(\frac{R}{r_0}\right)}. \tag{10}$$

in order to satisfy that the circulation of the total electric field between the wire and the cylinder must be equal to the potential difference,

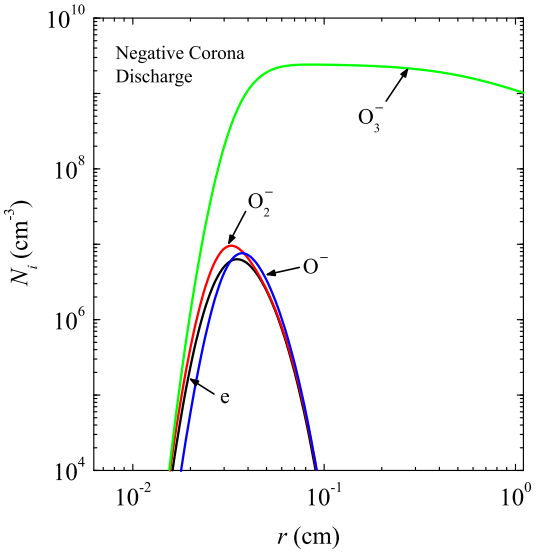

Fig. 10. Radial distribution of electrons and negative ions (negative corona) for $V = 6.8$ kV, $r_0 = 62.5$ μm and $R = 1.1$ cm (exact numerical solution).

$$V = \phi(r_0) - \phi(R) = \int_{r_0}^{R} E\,dr. \tag{11}$$

The electric field in the drift region must be obtained by solving Gauss equation,

$$\frac{1}{r}\frac{d}{dr}[rE] = \frac{e_0 N_p}{\varepsilon_0}, \tag{12}$$

where only the positive space charge, due to ions O_2^+, needs to be taken into account. However, since the density of ions and electrons affects negligibly the electric field in the ionization region, equation (12) is also satisfied in the entire inter-electrode gap. Besides, the electric current in the drift region is mostly transported by O_2^+,

$$I = 2\pi e_0 r L \mu_p N_p E. \tag{13}$$

Then, introducing (13) in (12), the governing equation for the electric field can be written as

$$\frac{1}{r}\frac{d}{dr}[rE] = \frac{I}{2\pi\varepsilon_0 r L \mu_p E}, \tag{14}$$

whose solution is

$$E = \sqrt{\frac{c^2}{r^2} + A^2}, \tag{15}$$

where $c = r_0\sqrt{E_0^2 - A^2}$ and $A = \sqrt{I/(2\pi\varepsilon_0 L\mu_p)}$. The parameter A accounts for the contribution of the space charge to the total electric field, which can be ignored in the vicinity the wire ($A \ll E_0$). Therefore, $c \approx E_0 r_0$ and (15) becomes (9) in the ionization region.

The value of the parameter c can be obtained from the integral of the electric field between the electrodes,

$$V = c\left[\ln\left(\frac{R}{r_0}\right) + \ln\left(\frac{1+\sqrt{1+(Ar_0/c)^2}}{1+\sqrt{1+(AR/c)^2}}\right) + \sqrt{1+\left(\frac{AR}{c}\right)^2} - \sqrt{1+\left(\frac{Ar_0}{c}\right)^2}\right], \tag{16}$$

Moreover, since $Ar_0/c \ll 1$, this equation can be simplified to

$$V = c\left[\ln\left(\frac{R}{r_0}\right) - \ln\left(1+\sqrt{1+\left(\frac{AR}{c}\right)^2}\right) + \ln(2) + \sqrt{1+\left(\frac{AR}{c}\right)^2} - 1\right]. \tag{17}$$

Using the experimental voltages and currents of the CV characteristic as input data, this equation allows the evaluation of the electric field strength E_0 on the wire surface. Then, it can be used in (15) to determine the distribution of the electric field in the whole inter-electrode space. A comparison between the electric field distributions calculated from the exact numerical model and from (15) is presented in Fig. 5. The agreement between the two results is excellent.

4.1.2. Electron density distribution

Within the ionization region, the electric field is very high and electron attachment can be neglected since, contrary to ionization, the attachment coefficient decreases with increasing the electric field. The ionization coefficient can be approximated by the following analytical expression [23]:

$$\alpha = A_1 \exp\left(-\frac{B_1}{E}\right), \tag{18}$$

where $A_1 = 8.97 \times 10^3$ cm^{-1} and $B_1 = 1.45 \times 10^5$ V/cm. Substituting (18) and (9) in (5), the equation governing for the electron density can be written as

$$\frac{1}{r}\frac{\mathrm{d}}{\mathrm{d}r}[rN_e\mu_e E] = -(A_1\exp(-B_2 r))N_e\mu_e E, \tag{19}$$

where $B_2 = B_1/(E_0 r_0)$.

Moreover, in the ionization region, the electric current is mainly transported by electrons, as it can be deduced from the numerical results presented in Fig. 3. The electron density at the wire surface can then be obtained from the experimental current voltage characteristic using (6), and it will be taken as a boundary condition for (19),

$$N_e(r_0) = \frac{I}{2\pi e_0 r_0 L \mu_e(E_0) E_0}. \tag{20}$$

The electron density distribution is finally determined by integrating (19) between r_0 and r

$$N_e(r) = \frac{I}{2\pi e_0 L}\frac{1}{b_1 r + b_2 r_0 E_0}\exp\left(-\frac{A_1}{B_2}\exp(-B_2 r_0)\right) \exp\left(\frac{A_1}{B_2}\exp(-B_2 r)\right). \tag{21}$$

where the electron velocity, $\mu_e E$, has been fitted as a linear function of the electric field from the experimental data available in [23],

$$\mu_e E = b_1 + b_2 E = b_1 + b_2\frac{E_0 r_0}{r} \tag{22}$$

with $b_1 = 1.42 \times 10^7$ cm/s and $b_2 = 257.3$ cm^2/(Vs). This linear fitting is only valid in the ionization region, where the electric field is sufficiently high.

Equation (21) predicts an exponential decrease of the electron density with the radial distance, which is in excellent agreement with the results obtained from the numerical simulation (Fig. 6).

4.1.3. Positive ion density distribution

As shown in Figs. 3 and 4, the electric current is sustained by electrons in the ionization region and by O_2^+ in the drift region. However, at the border between the two regions, both electrons and positive ions contribute to the transport of current. Therefore, the general expression for the density of positive ions can be obtained by substituting (15) and (21) in (6),

$$N_p(r) = \frac{I}{2\pi L e_0 E_0 r_0 \mu_p}\frac{1}{\sqrt{1+\left(\frac{Ar}{E_0 r_0}\right)^2}} \times\left[1-\exp\left(-\frac{A_1}{B_2}\exp(-B_2 r_0)\right)\exp\left(\frac{A_1}{B_2}\exp(-B_2 r)\right)\right] \tag{23}$$

Within the drift region, the transport of current is entirely due to positive ions, and (23) simplifies to

$$N_p(r) = \frac{I}{2\pi L e_0 E_0 r_0 \mu_p}\frac{1}{\sqrt{1+\left(\frac{Ar}{E_0 r_0}\right)^2}}. \tag{24}$$

That is, the spatial distribution of positive ions is only determined by the spatial distribution of the electric field.

In Fig. 7, the analytical solution (23) is compared with the exact numerical results. Clearly, the analytical solution constitutes an excellent approximation.

4.1.4. Temperature distribution

The augmentation of the gas temperature due to Joule heating has two effects on the electrical discharge. Firstly, it changes the transport coefficients of the gas and, secondly, it modifies the rate coefficients of many reactions that depend on temperature. The microscopic origin of the gas heating is the exchange of energy between charged species, accelerated by the electric field, and neutral species. The contribution of electrons to the gas heating can be neglected, since the energy transfer from electrons to heavy species is inefficient due to the differences in their masses. Furthermore, the ion O_2^+ is the dominant charged particle, as confirmed by the numerical results. Thus, the power density contributing to the gas heating can be reduced to the energy exchange between O_2^+ and neutral molecules,

$$P_h(r) \approx E(r) J_p(r), \tag{25}$$

where $J_p(r) = e_0\mu_p N_p(r) E(r)$ is the current density of positive ions.

The equation governing the gas temperature is then obtained by substituting (15) and (23) in (8),

$$-\frac{1}{r}\frac{\mathrm{d}}{\mathrm{d}r}\left[rk\frac{\mathrm{d}T}{\mathrm{d}r}\right] = \frac{I}{2\pi L}\frac{E(r)}{r}\left[1-\exp\left(-\frac{A_1}{B_2}\exp(-B_2 r_0)\right) \times\exp\left(\frac{A_1}{B_2}\exp(-B_2 r)\right)\right], \tag{26}$$

Two boundary conditions are required in order to integrate this equation. On the cylinder surface, the temperature is taken as constant and equal to the ambient temperature, since that electrode is in direct contact with the external air. On the wire, the gas is assumed to be in thermal equilibrium with this electrode. Therefore

$$T(R) = 298\ \mathrm{K}, \quad \left.\frac{\mathrm{d}T}{\mathrm{d}r}\right|_{r_0} = 0. \tag{27}$$

The exponential terms in (26) are only important in the ionization region, where the positive ion current tends to zero towards the wire. However, the extension of the ionization region is very small compared with the gap between the electrodes, and it can be neglected without introducing much error. Conversely, beyond the ionization region, the current is mainly transported by the positive ions. As shown in Section 4.1.1, the electric field in the drift region is affected by the presence of the positive space charge. However, in order to obtain a simple analytical solution for the gas temperature distribution, the electric field will be approximated by the Laplacian electric field (9) in the whole inter-electrode gap. Therefore, the temperature equation becomes,

$$-\frac{1}{r}\frac{\mathrm{d}}{\mathrm{d}r}\left[rk\frac{\mathrm{d}T}{\mathrm{d}r}\right] = \frac{c_1}{r^2}, \tag{28}$$

where $c_1 = E_0 r_0 I/(2\pi L)$. A straightforward integration of this equation gives

$$T(r) = T(R) + \frac{c_1}{2k}\ln\left(\frac{R}{r}\right)\ln\left(\frac{Rr}{r_0^2}\right). \tag{29}$$

This relation also reflects the dependence of temperature on the electric current and on the electric field on the wire through the parameter c_1.

Fig. 8 shows that the analytical solution (27) agrees qualitatively with the result obtained from the exact numerical model. The differences between the two solutions are due to the fact of having neglected the effect of the space on the electric field. The importance of the space charge increases with the applied voltage. Therefore, the agreement between the analytical solution and the exact numerical simulation is better at low applied voltages.

4.2. Negative corona discharge

In negative corona, the volume of the electrical discharge can be divided in three regions. The first region, surrounding the wire, is the ionization region. Due to the high intensity of the electric field, ionization is the dominant process occurring in the vicinity of the wire. The electrical discharge is sustained by secondary electron emission from the cathode produced by the impact of photons and positive ions. Since electron avalanches progress towards the anode, a maximum of electron density is reached at a certain distance from the wire. The region around that maximum is named the active region, because most of the chemical activity induced by the corona discharge occurs in that zone. Finally, the rest of the inter-electrode gap, up to the anode, constitutes the drift region, where electron attachment dominates over ionization owing to the low intensity of the electric field.

Similarly to positive corona, the numerical solution of (1)–(3) shows that a single ionic species is dominant in the ionization and drift regions: O_2^+ and O_3^-, respectively (Figs. 9 and 10). Therefore, a simplified model with only three species (electrons, O_2^+ and O_3^-) may be sufficient to reproduce the basic characteristics of the negative corona discharge in oxygen. The governing equations of the charged particles, electric field and temperature are then written as

$$\frac{1}{r}\frac{d}{dr}[rN_e\mu_e E] = (\alpha-\eta)N_e\mu_e E, \tag{30}$$

$$\frac{1}{r}\frac{d}{dr}\left[rN_p\mu_p E\right] = -\alpha N_e\mu_e E, \tag{31}$$

$$\frac{1}{r}\frac{d}{dr}[rN_n\mu_n E] = \eta N_e\mu_e E, \tag{32}$$

$$-\frac{1}{r}\frac{d}{dr}[rE] = \frac{e_0}{\varepsilon_0}(N_p - N_n - N_e), \tag{33}$$

$$-\frac{1}{r}\frac{d}{dr}\left[rk\frac{dT}{dr}\right] = EJ_{ion}, \tag{34}$$

where N_n is the number density of the negative ions (O_3^-).The above equations constitute a set of differential nonlinear coupled equations, which do not possess analytical solution. However, taking into account the information provided from more complex numerical simulations [15], approximate analytical solutions can be derived after introducing some simplifications.

4.2.1. Electric field distribution

According to the simulation results shown in Fig. 9, the electric is negligibly affected by the positive space charge in the ionisation region. Therefore, in that region, the electric field distribution can be described by means of (9), similarly to positive corona. On the contrary, the space charge is important in the drift region, which is dominated by ozone ions, O_3^-. Gauss equation and the current equation can be written in the drift region as follows:

$$\frac{1}{r}\frac{d}{dr}[rE] = \frac{e_0 N_n}{\varepsilon_0}, \tag{35}$$

$$I = 2\pi e_0 rL\mu_n N_n E, \tag{36}$$

where E and I represent the moduli of the electric field and current intensity, respectively. Since the density of the negative ions is insignificant in the ionisation region and in the active region, equation (35) can be considered valid in the whole inter-electrode space. This equation is formally identical to (12) for positive polarity. Thus, both share the same solution, and the electric field distribution can be expressed as

$$E = \sqrt{\frac{c^2}{r^2} + D^2}, \tag{37}$$

where $c \approx E_0 r_0$ and $D = \sqrt{I/(2\pi\varepsilon_0 L\mu_n)}$. Moreover, since $Dr_0 \ll c$, the relation between the parameter c and the electric potential will be analogous to (17),

$$V = c\left[\ln\left(\frac{R}{r_0}\right) - \ln\left(1+\sqrt{1+\left(\frac{DR}{c}\right)^2}\right) + \ln(2) + \sqrt{1+\left(\frac{DR}{c}\right)^2} - 1\right], \tag{38}$$

where V is the absolute value of the negative high voltage applied to the wire. Soria et al. and Feng, among others, have derived similar expression for the electric field and potential [11,24].

The applied voltage and measured current are used as input parameters in (38) to calculate the electric field on the wire surface. Then, the spatial distribution of the electric field can be determined using (37). In Fig. 11, the analytical solution is compared with the predictions of a complete numerical simulation. Both results are in good agreement.

4.2.2. Electron density distribution

In oxygen, the principal ionization reaction is

$$e + O_2 \rightarrow O_2^+ + e + e, \tag{R3}$$

while two different processes compete for the electron attachment

$$e + O_2 \rightarrow O^- + O, \tag{R4}$$

$$e + O_2 + O_2 \rightarrow O_2^- + O_2 \tag{R5}$$

However, as the ions O^- and O_2^- are drifted towards the anode, they are converted into O_3^- according to the following reactions:

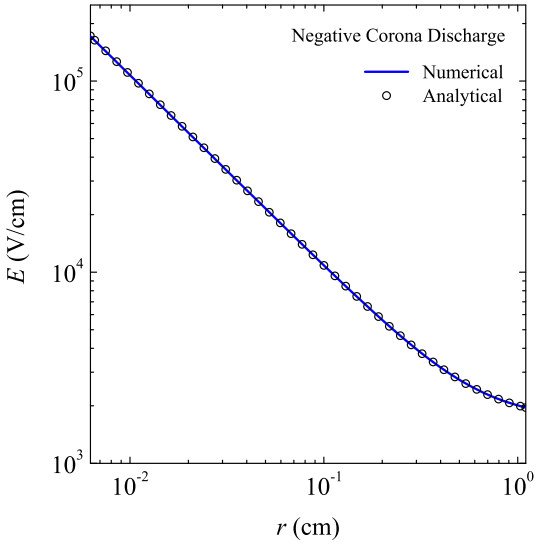

Fig. 11. Radial distribution of the electric field corresponding to V = 6.2 kV, r_0 = 62.5 μm and R = 1.1 cm (negative corona).

$$O_2^- + O_3 \rightarrow O_2 + O_3^-, \quad \text{(R6)}$$

$$O^- + O_3 \rightarrow O + O_3^-. \quad \text{(R7)}$$

Reactions (R6) and (R7) show that the equations governing the densities of charged and neutral particles are coupled. In (37), this fact was indirectly taken into account by using the mobility of O_3^-. However, in the case of gas flow, the dominant ion is not always O_3^-, but it depends on the value of the gas flow [25].

The attachment coefficient for reactions (R4) and (R5) can be interpolated from the data provided by Eliasson and Kogelschatz [23] as follows:

$$\eta = \alpha_1 + \alpha_2 E + \alpha_3 E^2 + \alpha_4 E^3, \quad \left(1.1 \times 10^4 \le E \le 2.0 \times 10^5 \text{ V/cm}\right) \quad (39)$$

where $\alpha_1 = 100.7$ cm^{-1}, $\alpha_2 = -1.27 \times 10^{-3}$ V^{-1}, $\alpha_3 = 6.818 \times 10^{-9}$ cm/V^2 and $\alpha_4 = -1.416 \times 10^{-14}$ cm^2/V^3.

The electron density is only important in the active region of the corona discharge. According to the numerical simulation results, the electric field in that region can be satisfactorily approximated by the Laplacian electric field (9). Therefore, the attachment coefficient will be expressed as

$$\eta = a_1 + \frac{a_2}{r} + \frac{a_3}{r^2} + \frac{a_4}{r^3}, \quad (40)$$

where $a_1 = \alpha_1$, $a_2 = \alpha_2 E_0 r_0$, $a_3 = \alpha_3 (E_0 r_0)^2$ and $a_4 = \alpha_4 (E_0 r_0)^3$.

Substituing (18) and (40) in (30) and integrating along the radial coordinate, the following expression for the electron density is obtained,

$$N_e(r) = N_e(r_0) \frac{\mu_e(r_0) E_0}{\mu_e E} \left(\frac{r_0}{r}\right)^{a_2+1} \times \exp\left[\frac{A_1}{B_2}(\exp(-B_2 r_0) - \exp(-B_2 r)) - a_1(r - r_0) + a_3\left(\frac{1}{r} - \frac{1}{r_0}\right) + \frac{a_4}{2}\left(\frac{1}{r^2} - \frac{1}{r_0^2}\right)\right], \quad (41)$$

where the ratio of electron velocities, $\mu_e(r_0)E_0/\mu_e E$, can be evaluated using (22). Only the electron density on the wire, $N_e(r_0)$, remains to be determined. This will be done in Section 4.2.4, after deriving the expression for the positive ion density.

The relation (41) exhibits a sharp increase of the electron density near the wire, due to the ionization process, followed by a rapid decrease caused by the dominance of attachment over ionization. Fig. 12 shows that the analytical solution of the electron density is in fair agreement with the numerical simulation results. The small difference between the two methods is mainly due to having ignored reactions of secondary importance in the analytical solution.

4.2.3. Positive ion density distribution

The electric current is mainly transported by the positive ions (O_2^+) in the ionization region. Therefore, the current on the wire surface is given by

$$I \approx 2\pi e_0 r_0 L \mu_p N_p(r_0) E_0, \quad (42)$$

Integrating (31) and using (42) as a boundary condition for the positive ion density on the wire, the spatial distribution of positive ions can be expressed as

$$N_p(r) = \frac{1}{r_0 E_0 \mu_p}\left[\frac{I}{2\pi L e_0} - A_1 r_0 E_0 \int_{r_0}^{r} \mu_e N_e \exp(-B_2 r) dr\right], \quad (43)$$

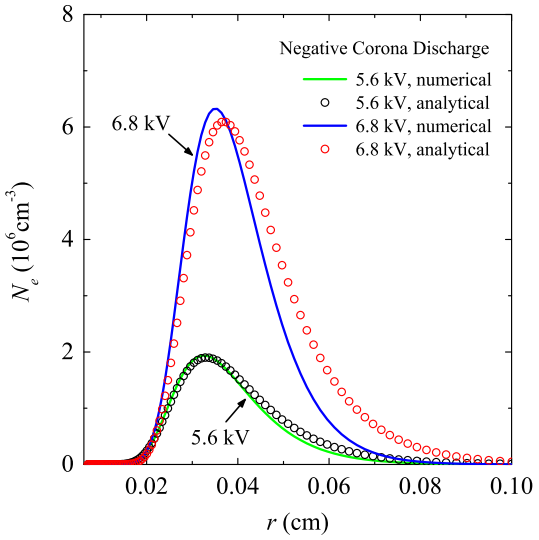

Fig. 12. Radial distribution of the electron density for $r_0 = 62.5$ μm and $R = 1.1$ cm (negative corona).

Unfortunately, the evaluation of the integral must be done numerically, after substituting (41) in (43). The predictions of this semi-analytical relation and of the numerical simulation are compared in Fig. 13. Only minor differences are observed between both results.

4.2.4. Electron density on the wire surface

In order to evaluate the electron density distribution in (41), the electron density on the wire surface must be first determined. In the active region of the corona discharge, the electron current reaches a maximum when the ionisation coefficient equals the attachment coefficient. According to (18) and (39), this happens for an electric field strength of about $E_1 = 30$ kV/cm, and at a radial coordinate $r_1 \approx E_0 r_0 / E_1$. In such a place, the electric currents due to positive and negative ions are similar, $J_n(r_1) \approx J_p(r_1)$, and the total current can be written as

$$I = 2\pi e_0 r_1 L\left(J_e(r_1) + 2J_p(r_1)\right) = 2\pi e_0 r_1 L\left(\mu_e(r_1) N_e(r_1) + 2\mu_p N_p(r_1)\right) E(r_1), \quad (44)$$

This equation can be used as a boundary condition to determine the electron density on the wire surface. Substituting (41) and (43) in (44) leads to

$$N_e(r_0) = \frac{I}{2\pi L e_0 \mu_e(r_0) E_0} \frac{1}{2A_1\left[\int_{r_0}^{r_1} r \exp(-B_2 r) f(r) dr\right] - r_1 f(r_1)}, \quad (45)$$

where

$$f(r) = \left(\frac{r_0}{r}\right)^{a_2+1} \exp\left[\frac{A_1}{B_2}(\exp(-B_2 r_0) - \exp(-B_2 r)) - a_1(r - r_0) + a_3\left(\frac{1}{r} - \frac{1}{r_0}\right) + \frac{a_4}{2}\left(\frac{1}{r^2} - \frac{1}{r_0^2}\right)\right]. \quad (46)$$

4.2.5. Negative ion density distribution

As discussed in Section 4.2.2, the ions O^- and O_2^- are converted into O_3^- through reactions (R6) and (R7). The radial distribution of O_3^- is then obtained by integrating (32)

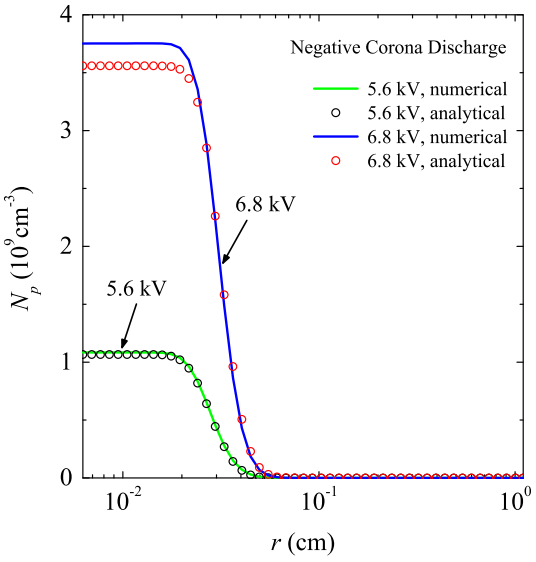

Fig. 13. Radial distribution of the positive ion (O_2^+) density for $r_0 = 62.5$ μm and $R = 1.1$ cm (negative corona).

$$N_n(r) = \frac{1}{\mu_n r\sqrt{\frac{c^2}{r^2}+D^2}} \int_{r_0}^{r} r\left(a_1+\frac{a_2}{r}+\frac{a_3}{r^2}+\frac{a_4}{r^3}\right) N_e \mu_e E \, dr. \quad (47)$$

Similarly to the number density of positive ions, the evaluation of the integral must be done numerically, after substituting (41) in (47). However, in the drift region, where the electric current (36) is only transported by O_3^-, the density of negative ions can also be expressed as

$$N_n(r) = \frac{I}{2\pi L e_0 \mu_n r E} = \frac{I}{2\pi L e_0 \mu_n r\sqrt{\frac{c^2}{r^2}+D^2}}. \quad (48)$$

In Fig. 14, the numerical simulation results are compared with the predictions of the semi-analytical relation (47).

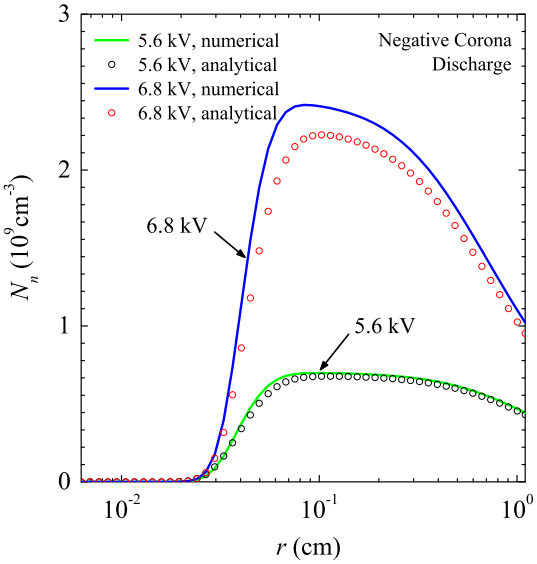

Fig. 14. Radial distribution of the negative ion (O_3^-) density for $r_0 = 62.5$ μm and $R = 1.1$ cm (negative corona).

4.2.6. Temperature distribution

In the negative corona, the exchange of energy between the ions O_2^+ and the gas molecules constitutes the main process for the gas heating. Therefore, the power density contributing to the gas heating can be expressed as

$$P_h(r) \approx E(r) J_p(r) = E_0 r_0 \frac{I}{2\pi L r^2}, \quad r_0 \le r \le r_i \quad (49)$$

The validity of this expression is restricted to the ionization region, where the positive ion current is important. Beyond the ionization region, that is, in the active and drift regions, the electric current is mainly transported by electrons and negative ions, respectively. Since the electric field is significantly lower in the drift region, the exchange of kinetic energy between the negative carriers and the gas molecules is insufficient to cause an important gas heating. Thus, the power density contributing to the gas heating will be negligible,

$$P_h(r) \approx 0, \quad r_i \le r \le R. \quad (50)$$

Substitutions of (49) and (50) in (34) leads to

$$-\frac{1}{r}\frac{d}{dr}\left[rk\frac{dT}{dr}\right] \approx \frac{c_1}{r^2}, \quad r_0 \le r \le r_i \quad (51)$$

$$-\frac{1}{r}\frac{d}{dr}\left[rk\frac{dT}{dr}\right] \approx 0, \quad r_i \le r \le R, \quad (52)$$

where $c_1 = E_0 r_0 I/(2\pi L)$.

To integrate (51) and (52), the same boundaries as for the positive corona discharge are taken on the wire and on the outer electrode. At the border of the ionization region, the continuity of temperature and of the heat flux is imposed,

$$T(R) = 298 \text{ K}, \left.\frac{dT}{dr}\right|_{r_0} = 0, \; T(r_{i-}) = T(r_{i+}), \left.\frac{dT}{dr}\right|_{r_i^-} = \left.\frac{dT}{dr}\right|_{r_i^+}. \quad (53)$$

The analytic solutions of (51) and (52) are then

$$T(r) = \frac{c_1}{k}\left[\frac{1}{2}\ln\left(\frac{r_i}{r}\right)\ln\left(\frac{r_i r}{r_0^2}\right)+\ln\left(\frac{r_0}{r_i}\right)\ln\left(\frac{r_i}{R}\right)\right]+T(R), \quad r_0 \le r \le r_i \quad (54)$$

$$T(r) = \frac{c_1}{k}\ln\left(\frac{r_0}{r_i}\right)\ln\left(\frac{r}{R}\right)+T(R), \quad r_i \le r \le R. \quad (55)$$

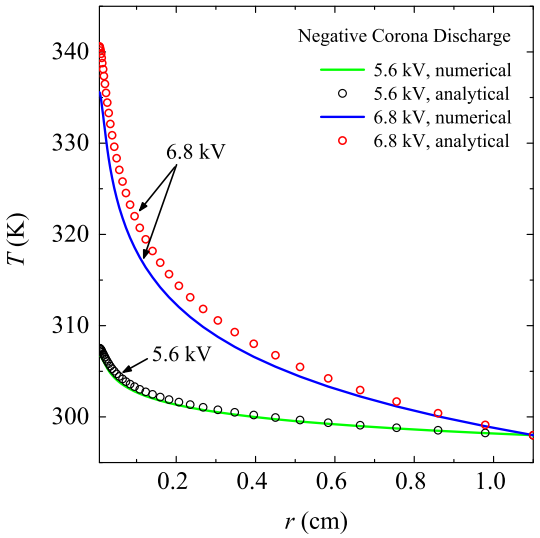

Fig. 15. Radial distribution of temperature corresponding to $r_0 = 62.5$ m and $R = 1.1$ cm (negative corona).

According to the previous results, the value for r_i can be taken as $r_i \approx 0.03$ cm. At this position, the power density has decreased about 20 times from its value on the surface of the wire. In Fig. 15, the radial distribution of temperature given by the relations (54) and (55) is compared with the result of the numerical simulation. The agreement between both results is quite satisfactory. As for the positive corona, the gas temperature is controlled by the parameter c_1, which depends on the product $E_0 l$.

5. Conclusion

In this paper, analytical expressions of the electric field, charged particles and temperature in the inter-electrode space have been obtained for both positive and negative wire-to-cylinder DC corona discharge in pure oxygen. The analytical solutions have been derived using a simplified fluid model of the corona discharge, and solving Gauss equation, the continuity equations of charged particles and the heat conduction equation. A priority objective of this work was to keep the model as simple as possible, so that the analytical solutions were straightforward. The voltages and current intensities measured in experiments have been used as input data to obtain the analytical expressions. The simplifications introduced in the analytical model have been justified on the basis of the results provided by a more complete numerical model of the corona discharge. The agreement between the analytical solutions and the exact numerical results is very satisfactory. Even though some important processes of the corona discharge, like photoemission and the photoionisation, have apparently been ignored in the analytical model, they have been taken into account indirectly by using the experimental current–voltage characteristic as a boundary condition of the governing equations. The averaged gas temperature caused by Joule heating was found to depend on the product of the electric current and the electric field on the wire surface. Finally, the present analytical approach can also be useful in other gases, apart from oxygen, that produce stable corona discharge, and it may helps to understand the physics of corona discharge in applications like decomposition of gaseous pollutants, sterilization, polymer treatment, ozone production, etc.

Acknowledgements

This work has been supported by Agence Nationale pour le Développement de la Recherche Universitaire (Algeria) in the frame of project PNR, and by the Consejería de Innovación, Ciencia y Empresa (Junta de Andalucía, Spain) within the European Regional Development Fund project P09-FQM-4983.

References

[1] J.J. Lowke, R. Morrow, Theoretical analysis of removal of oxides of sulfur and nitrogen in pulsed operation of electrostatic precipators, IEEE Transactions on Plasma Sciences 23 (1995) 661–671.
[2] M.L. Balmer, G. Fisher, J. Hoard (Eds.), Non-thermal Plasma for Exhaust Emission Control: NOx, HC, and Particulates, Society of Automotive Engineers, Inc, Warrendale, PA, 1999.
[3] M. Yamamoto, M. Nishioka, M. Sadakata, Sterilization by H_2O_2 droplets under corona discharge, Journal of Electrostatics 55 (2002) 173–187.
[4] T. Hammer, Application of plasma technology in environmental techniques, Contributions to Plasma Physics 39 (1999) 441–462.
[5] Y. Akishev, S. Kroepke, J. Behnisch, A. Hollander, A. Napartovich, N. Trushkin, Non-thermal plasma treatment of polymer films and fabrics based on a glow discharge at atmospheric pressure, in: H. Wagner, J.F. Behnke, G. Babucke (Eds.), Proceedings of the International Symposium on High Pressure Low Temperature Plasma Chemistry, vol. 2, 2000, pp. 481–485 Greifswald, Germany.
[6] J.A. Dorsey, J.H. Davidson, Ozone production in electrostatic air cleaners with contaminated electrodes, IEEE Transaction on Industry Applications 30 (1994) 370–376.
[7] G.S.P. Castle, I.I. Inculet, N.I. Burgess, Ozone generation in positive corona electrostatic precipitators, IEEE Transactions on Industry and General Applications IGA-5 (1969) 489–496.
[8] J.S. Chang, P.A. Lawless, T. Yamamoto, Corona discharge processes, IEEE Transactions on Plasma Sciences 19 (1991) 1152–1166.
[9] F. Pontiga, C. Soria, A. Castellanos, J.D. Skanly, An study of ozone generation by negative corona discharge through different plasma chemistry models, Ozone Science and Engineering 24 (2002) 447–462.
[10] J.H. Chen, J.H. Davidson, Electron density and energy distributions in the positive DC corona: interpretation for corona-enhanced chemical reactions, Plasma Chemistry and Plasma Processing 22 (2002) 199–224.
[11] C. Soria, F. Pontiga, A. Castellanos, Plasma chemical and electrical modelling of a negative dc corona in pure oxygen, Plasma Sources Science and Technology 13 (2004) 95–107.
[12] K. Adamiak, P. Atten, Simulation of corona discharge in point–plane configuration, Journal of Electrostatics 61 (2004) 85–98.
[13] J. Zhang, K. Adamiak, G.S.P. Castle, Numerical modeling of negative-corona discharge in oxygen under different pressures, Journal of Electrostatics 65 (2007) 174–181.
[14] J. Zhang, K. Adamiak, A multi-species DC stationary model for negative corona discharge in oxygen; point-plane configuration, Journal of Electrostatics 65 (2007) 459–464.
[15] K. Yanallah, F. Pontiga, A. Fernandez-Rueda, A. Castellanos, A. Belasri, Ozone generation by negative corona discharge: the effect of Joule heating, Journal of Physics D: Applied Physics 41 (2008) 195206 (8 pp).
[16] P. Wang, J. Chen, Numerical modelling of ozone production in a wire-cylinder corona discharge and comparison with a wire-plate corona discharge, Journal of Physics D: Applied Physics 42 (2009) 035202 (8 pp).
[17] K. Yanallah, F. Pontiga, A. Fernandez-Rueda, A. Castellanos, Experimental investigation and numerical modeling of positive corona discharge: ozone generation, Journal of Physics D: Applied Physics 42 (2009) 065202 (8 pp).
[18] R.G. Stearns, The positive corona in air: a simplified analytic approach, Journal of Applied Physics 66 (1989) 2899–2913.
[19] B. Held, R. Peyrous, Analytic calculations of ozone concentration in an oxygen-fed wire-to-cylinder ozonizer and comparison with the Vasil'ev relation, The European Physical Journal Applied Physics 4 (1998) 73–86.
[20] T. Mikoviny, M. Kocan, S. Matejik, N.J. Mason, J.D. Skanly, Experimental study of corona discharge in pure carbon dioxide and its mixture with oxygen, Journal of Physics D: Applied Physics 37 (2004) 64–73.
[21] A.A. Belevtsev, L.M. Biberman, On the theory of corona discharge, Beiträge aus der Plasmaphysik 23 (1983) 313–330.
[22] J. Chen, J.H. Davidson, Model of the negative dc corona plasma comparison to the positive DC corona plasma, Plasma Chemistry and Plasma Processing 23 (2003) 83–102.
[23] B. Eliason, U. Kogelschatz, Basic Data for Modelling of Electrical Discharges in Gases: Oxygen Technical Report KLR 86-11C, Brown Boveri, 1986.
[24] J.Q. Feng, An analysis of corona currents between two concentric cylindrical electrodes, Journal of Electrostatics 46 (1999) 37–48.
[25] K. Yanallah, F. Pontiga, A. Fernandez-Rueda, A. Castellanos, A. Belasri, Experimental Characterization and Numerical Modeling of a Wire-to-cylinder Corona Discharge Ozonizer Annual Report Conference on Electrical Insulation and Dielectric Phenomena, Vancouver, British, Columbia, CA (2007) pp. 667–670.